Provided for non-commercial research and education use.
Not for reproduction, distribution or commercial use.

This article appeared in a journal published by Elsevier. The attached copy is furnished to the author for internal non-commercial research and education use, including for instruction at the authors institution and sharing with colleagues.

Other uses, including reproduction and distribution, or selling or licensing copies, or posting to personal, institutional or third party websites are prohibited.

In most cases authors are permitted to post their version of the article (e.g. in Word or Tex form) to their personal website or institutional repository. Authors requiring further information regarding Elsevier's archiving and manuscript policies are encouraged to visit:

http://www.elsevier.com/copyright

Author's personal copy

doi:10.1016/j.jmb.2010.09.055 J. Mol. Biol. (2010) 404, 493–505

Contents lists available at www.sciencedirect.com

Journal of Molecular Biology

journal homepage: http://ees.elsevier.com.jmb

Gradual Adaptive Changes of a Protein Facing High Salt Concentrations

Nicolas Coquelle[1], Romain Talon[1], Douglas H. Juers[1,2], Éric Girard[1], Richard Kahn[1] and Dominique Madern[1]*

[1]*IBS, Institut de Biologie Structurale Jean-Pierre Ébel, Extremophilic and Large Molecular Assemblies Team, UMR 5075, CEA, CNRS, Université Joseph Fourier, 41 rue Jules Horowitz, F-38027 Grenoble, France*
[2]*Department of Physics, Whitman College, Walla Walla, WA 99362, USA*

Received 9 July 2010;
received in revised form
22 September 2010;
accepted 24 September 2010
Available online
1 October 2010

Edited by G. Schulz

Keywords:
halophilic;
malate dehydrogenase;
protein adaptation;
stability;
solubility

Several experimental techniques were applied to unravel fine molecular details of protein adaptation to high salinity. We compared four homologous enzymes, which suggested a new halo-adaptive state in the process of molecular adaptation to high-salt conditions. Together with comparative functional studies, the structure of malate dehydrogenase from the eubacterium *Salinibacter ruber* shows that the enzyme shares characteristics of a halo-adapted archaea-bacterial enzyme and of non-halo-adapted enzymes from other eubacterial species. The *S. ruber* enzyme is active at the high physiological concentrations of KCl but, unlike typical halo-adapted enzymes, remains folded and active at low salt concentrations. Structural aspects of the protein, including acidic residues at the surface, solvent-exposed hydrophobic surface, and buried hydrophobic surface, place it between the typical halo-adapted and non-halo-adapted proteins. The enzyme lacks inter-subunit ion-binding sites often seen in halo-adapted enzymes. These observations permit us to suggest an evolutionary pathway that is highlighted by subtle trade-offs to achieve an optimal compromise among solubility, stability, and catalytic activity.

© 2010 Elsevier Ltd. All rights reserved.

Introduction

Halophilic microorganisms inhabit extremely saline environments, up to NaCl saturation. These microbes have selected various strategies of adaptation in order to cope with the resulting strong osmotic pressure.[1] One strategy is to maintain a low cytoplasmic salt concentration using salt-exclusion mechanisms together with the synthesis and/or accumulation of compatible solutes (osmolytes).[1] Halophilic organisms that use this strategy (typically eubacteria and higher organisms) have efficient transmembrane ion-selective pumps as well as specific pathways for osmolyte synthesis. A second strategy involves KCl accumulation at molar concentrations in the cytoplasm to counterbalance the external osmotic pressure. This strategy is typical of extreme halophilic archaea but was also recently discovered for the first time in a eubacterial species, *Salinibacter ruber* (*Sr*), which inhabits the same natural environment as halophilic archaea.[2] Whereas osmolytes typically have only small effects on enzyme stability and catalysis, high salt concentrations are generally deleterious to enzyme function.[3] Nevertheless, enzymes from halophilic cells have evolved to maintain solubility, catalytic efficiency, and structural stability in high concentrations of KCl, all necessary for proper function.[4,5]

*Corresponding author. E-mail address: Dominique.Madern@ibs.fr.

Abbreviations used: OAA, oxaloacetate; MalDH, malate dehydrogenase; LDH, lactate dehydrogenase; *Ca*, *Chloroflexus aurantiacus*; *Sr* (halophilic bacterium), *Salinibacter ruber* (halophilic bacterium); *Hm*, *Haloarcula marismortui* (halophilic archaea); *Tt*, *Thermus thermophilus*; AUC, analytical ultracentrifugation; PDB, Protein Data Bank.

0022-2836/$ - see front matter © 2010 Elsevier Ltd. All rights reserved.

Author's personal copy

Work on several protein systems over the last 15 years has uncovered three general features of molecular adaptation via the KCl accumulation strategy.[6–10] First, halophilic proteins from extreme archaea are very acidic, with a mean calculated p*I* value of 5 for proteomes of various halophilic species. Crystal structures of several proteins from halophilic archaeal cells with KCl-rich cytoplasms have shown their surfaces to be rich in acidic residues.[11] Second, many halophilic proteins have specific ion-binding sites, often at subunit interfaces. Third, there is often a reduction of hydrophobic content of the protein, on the folded surface as well as buried in the core. This occurs, in some cases, via the substitution of large hydrophobic residues for small ones and, in other cases, concomitantly with the reduction of the number of lysine residues. A recent site-directed mutagenesis study underscored the decrease of a protein's solvent-accessible area as an important mechanism for halo-adaptation.[12]

One of the most extensively studied groups of proteins with respect to halo-adaptation is the family of lactate dehydrogenase (LDH)-like malate dehydrogenases (MalDHs).[13] A halophilic version of MalDH from the archaeon *Haloarcula marismortui* (*Hm*) is a 130-kDa homotetramer, bearing each of the three adaptive signatures described above.[14,15] The solvent interactions, stability, and weak protein–protein interactions of *Hm* MalDH in the presence of various salts have been studied in detail previously.[16] At high physiological salt concentrations, the solvation shell of this very acidic enzyme has a slightly higher concentration of salt than that of a non-halophilic protein, whereas its water binding capacity is comparable to that of a non-halophilic protein.[16,17] With a solvation shell similar to bulk solvent, the protein can remain soluble in high salt concentrations. At low salt concentrations (below 2 M KCl), the *Hm* MalDH enzyme dissociates and unfolds.[4,5] The stability of *Hm* MalDH depends on the types and concentrations of cations and anions present in the buffer.[15] Anions appear to control stability via a few strong binding sites, whereas cations play a dual role through both weak binding sites and hydration effects.

The crystal structure of *Hm* MalDH shows the surface of the tetramer to be enriched in acidic residues.[7,18] Complex salt bridges occur across the monomeric interfaces that form the tetramer, and each tetramer contains two sodium-binding sites and eight chloride-binding sites. Non-halophilic orthologs of LDH-like MalDH from several eubacteria have also been studied,[19] but to date, there is little information to provide a link between these enzymes and the halophilic *Hm* MalDH. To assess if an identical evolutionary constraint (high cytoplasmic KCl concentration) induced an adaptive response similar to that observed in *Hm* MalDH, we analyzed the molecular properties of LDH-like MalDH from the halophilic bacterium *Sr*.

Purification of this enzyme was described previously, and some of its biochemical properties were investigated. However, this characterization was only partial as the sequence and three-dimensional structure remained unknown at that time.[20] In the present study, we report the crystal structure of the enzyme at a resolution of 1.55 Å and analyze the solution behavior in different salt conditions. In addition, we extend and enhance this characterization by including two other non-halophilic counterparts. Our comparative work indicates that the *Sr* MalDH corresponds to a newly described acclimation state of an enzyme adapting to high-salt conditions.

Results

Comparison strategy

We explored the effects of KCl on (i) the conformational stability, (ii) weak protein–protein interactions that control solubility, and (iii) enzymatic activities of the various halophilic and non-halophilic homologs from the LDH and LDH–MalDH superfamily. We analyzed the data with respect to the available structural information including consideration of the structural features previously described as important for halophilic adaptation (Fig. 1). The halophilic LDH-like MalDHs were from the bacterium *Sr* and the archaeon *Hm*, while the non-halophilic enzymes were the bacteria *Chloroflexus aurantiacus* (*Ca*) LDH-like MalDH and *Thermus thermophilus* (*Tt*) LDH.[21]

Crystal structure of *Sr* MalDH

The structure of *Sr* MalDH enzyme was determined at 1.55 Å resolution using molecular replacement (Table 1). The asymmetric unit contains a 314-residue monomer, with the physiological tetramer obeying the crystal 222 symmetry (Fig. 1). The final *Sr* MalDH model shows a fold previously observed for enzymes of the LDH–MalDH family, composed of two topological domains: a dinucleotide-binding domain and a catalytic domain.[7,18,19] Sequence identities between *Sr* MalDH and *Tt* LDH, between *Sr* MalDH and *Ca* MalDH, and between *Sr* MalDH and *Hm* MalDH are 35%, 53%, and 34%, respectively, while structural similarities, as measured by RMSD, are 1.21 , 0.60 , and 1.07 Å, respectively, for 210, 258, and 216 superimposed C^{α} atoms. Weak electron density occurs in two short regions of the *Sr* enzyme. Consequently, the model does not include the two carboxy-terminal residues or, as frequently observed in crystal structures of LDHs and MalDHs,

Author's personal copy

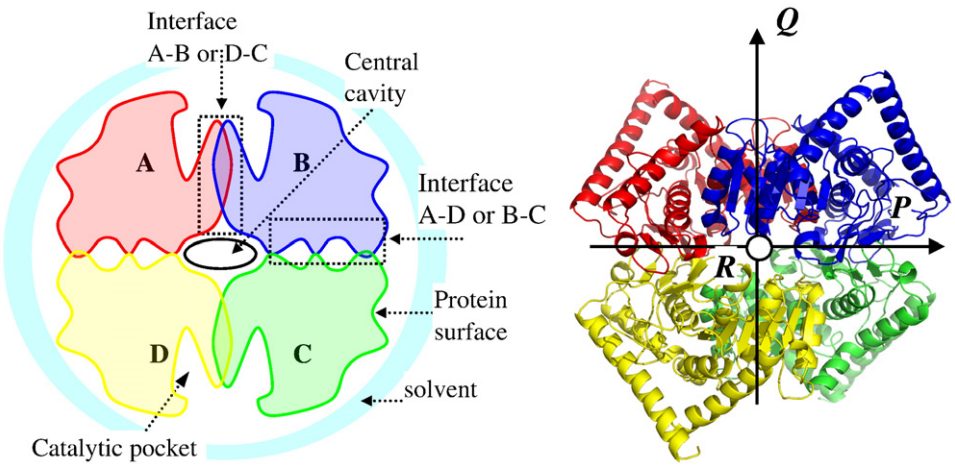

Fig. 1. Left panel: Schematic drawing of the tetrameric state of LDH and LDH-like MalDH. Each monomer is labeled A, B, C, or D. In the present study, several biochemical properties of the halophilic *Sr* LDH-like MalDH are analyzed with respect to several structural features: the nature of the various interfaces (A–B or B–C) that play a role in the quaternary structure, the protein surface, and the catalytic pocket. Right panel: C^{α} ribbon drawing of the tetrameric *Sr* enzyme. The tetramer has three dyads named P, Q, and R following the convention of Rossmann.

a flexible loop (residues 101–108 for *Sr* MalDH). The final *Sr* MalDH model also includes 340 water molecules per monomer with no ions.

Sr MalDH shows the conformational stability of a non-halophilic protein

The conformational stabilities of the four enzymes after a 24-h incubation at 25 °C in various KCl concentrations were compared. Data for *Tt* LDH and *Ca* MalDH were measured here, whereas data from *Sr* MalDH and *Hm* MalDH were taken from previous studies.[18,20] Both *Tt* LDH and *Ca* MalDH show a salt-independent stability, as expected for non-halophilic proteins (Fig. 2a and b). As was shown previously,[20] *Sr* MalDH is also stable over the whole KCl range (Fig. 2c), whereas the halophilic *Hm* MalDH unfolds below 2 M KCl (Fig. 2d). Previous measurements of the *Sr* MalDH quaternary assembly using analytical ultracentrifugation (AUC) showed that the enzyme is still tetrameric after 24 h of incubation at low salt,[4,6] which was repeated here. After the first AUC data acquisition on *Tt* LDH, *Ca* MalDH, and *Sr* MalDH at low KCl (0.05 M), the cell contents were homogenized and a second measurement was performed. The AUC results were identical before and after incubation, showing again that these enzymes are stable (data not shown).

The low-salt unfolding for *Hm* MalDH, which is well documented,[4,6] is due to the presence of ion-binding sites at the tetramer interfaces. A putative sodium-binding site at a dimer interface (two sites per tetramer) and two different chloride-binding sites (eight sites per tetramer) contribute to the native assembly.[7,18] The role of the chloride-binding sites in the stabilization and association of the enzyme has been well established using site-directed mutagenesis.[18,22]

Table 1. Crystal parameters, data collection, and refinement statistics

	Sr MalDH
Data collection	
ESRF beam line	BM30–ID29
Wavelength (Å)	0.9797–0.9320
Resolution range (Å)	33–1.55 (1.60–1.55)
Space group	*I*222
Cell dimensions (Å)	
a	76.11
b	87.72
c	100.45
R_{merge}	0.083 (0.499)
$\langle I/\sigma I \rangle$	11.4 (2.2)
Redundancy	6.4 (4.0)
Completeness (%)	97.5 (93.2)
Refinement	
Resolution (Å)	33–1.55
R_{work}/R_{free}	0.168/0.192
Number of atoms	
Protein	2360
Waters	340
Mean *B*-factor (Å^2)	
Protein	28.9
Water	41.7
RMSD	
Bond length (Å)	0.013
Bond angle (°)	1.33
Ramachandran statistics (%)	
Favorable	98.7
Allowed	1.3

Values in parentheses correspond to the highest-resolution shell.

Author's personal copy

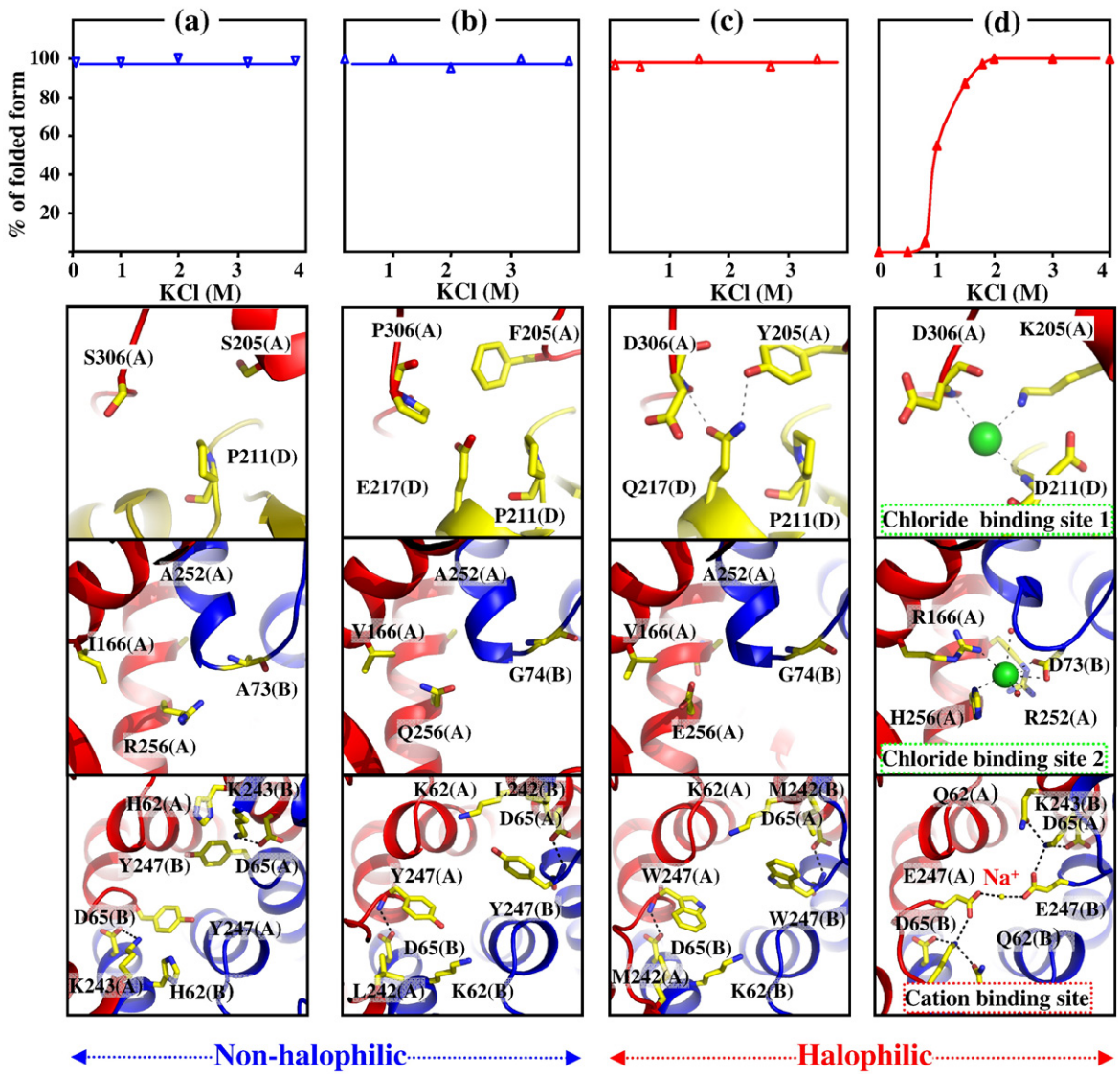

Fig. 2. Graphs: The effect of salt concentration on the conformational stability of *Tt* LDH (a), *Ca* (b), *Sr* (c), and *Hm* MalDH (d). Pictures: Close-up view of structures at positions that allow comparison of the most important amino acid substitutions involved in the salt-concentration-dependent stability. Non-halophilic enzymes (*Tt* LDH and *Ca* MalDH) and halophilic *Sr* MalDH lack the specific ion-binding sites that control the salt-concentration-dependent stability of the *Hm* enzyme: compare positions equivalent to those of *Hm* chloride-binding site no. 1 (four sites per tetramer) (top row), *Hm* chloride-binding site no. 2 (four sites per tetramer) (middle row), and *Hm* cation-binding site (two sites per tetramer) (bottom row). The monomers are colored according to Fig. 1.

At the positions equivalent to two different intersubunit chloride-binding sites (CB1 and CB2) of *Hm* MalDH (between monomers A and D), *Sr* MalDH does not contain ions and is more similar to its non-halophilic orthologs from *Tt* and *Ca*, which also lack bound ions (Fig. 2). According to structural criteria (ion–ligand distances and opposing negative charges), a sodium ion was identified in *Hm* MalDH between monomers A and B.[7,18] The same location in *Sr* MalDH is occupied by hydrophobic amino acids, suggesting that the cation-binding site is absent (Fig. 2). As lithium chloride, a non-physiological salt, was a constituent of the crystallization solutions used with *Sr* MalDH, a careful inspection of the solvent structure was conducted to detect these ions. Non-protein positive peaks (larger than 3 σ) in difference Fourier maps were modeled as water molecules. Due to the larger number of electrons for Cl^- (17) *versus* water (10), large positive peaks would be expected in the difference Fourier maps if chloride ions were bound to the protein. Moreover, a water molecule modeled in place of a chloride ion should have a very low *B*-factor compared to those of neighboring residues. No

Author's personal copy

chloride ions were identified in our model by using these criteria. Lithium ion–protein interactions can be characterized by interatomic distances and coordination geometries.[23] Based on high-resolution protein structures (<1.5 Å resolution), the distances between a bound lithium ion and its oxygen or nitrogen atom ligands are generally in the 1.8- to 2. 0-Å range. None of the water molecules bound to *Sr* MalDH showed such interaction distances, suggesting the absence of bound lithium ions. To distinguish water molecules from sodium ions (which differ by only a single electron), we considered the coordination geometry of solvent molecules with coordination number greater than 4, as well as structural similarities or differences between *Sr* and *Ca* MalDHs. No water molecule fulfilled the criteria to be assigned as a sodium ion. Finally, we tried to look for sites with unfavorable interactions such as negatively charged residues facing each other, as was used to identify a potential cation-binding site in *Hm* MalDH.[7,18] However, no such structural motif was observed in *Sr* MalDH. The other interactions at the various monomeric interfaces that build up the tetramer are very similar between *Sr* and *Ca* MalDH. The lack of both bound ions and unfavorable interactions explain why the conformational stability of *Sr* MalDH at low salt concentrations is similar to that of a non-halophilic ortholog.

Changes in surface properties control solubility

Effects of salt on the solubility of proteins are well studied.[24] For a protein to be soluble, the concentra-

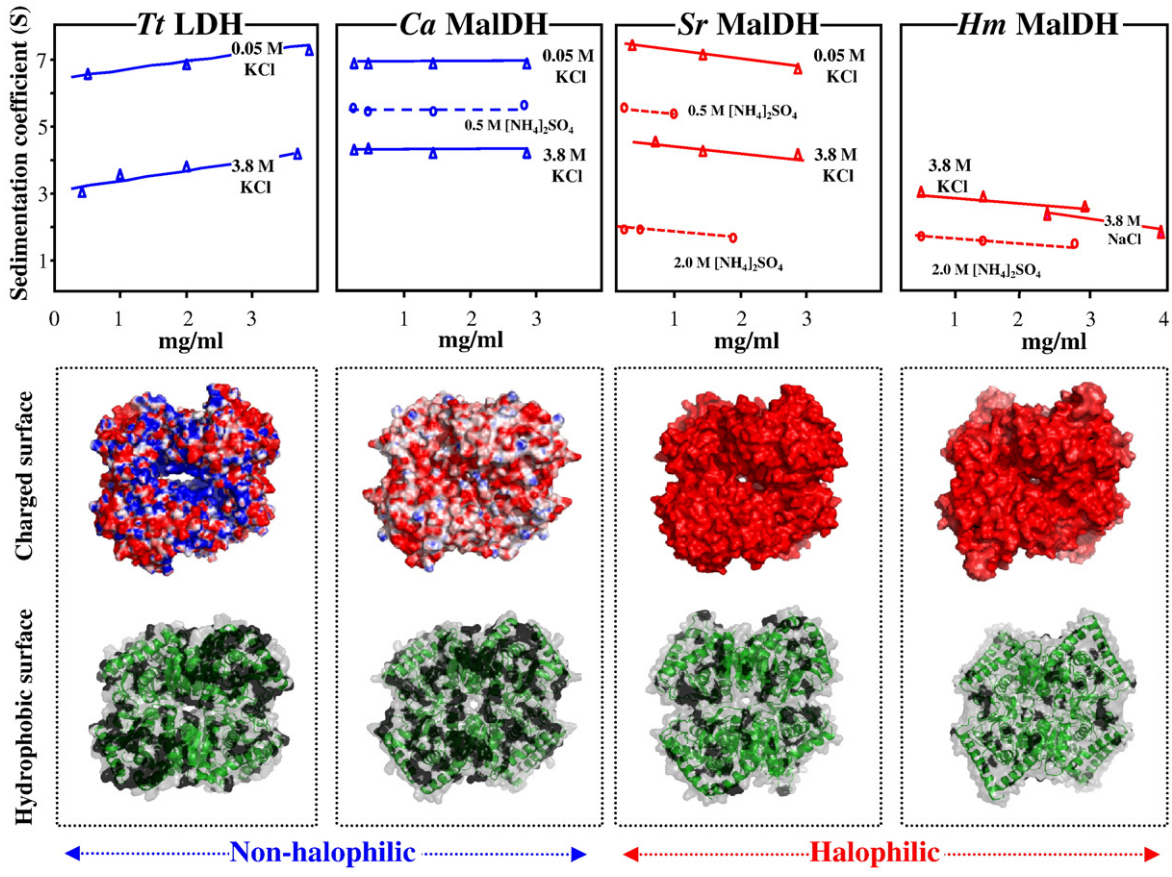

Fig. 3. Graphs: Variation of the experimental sedimentation coefficient (S_{exp}) at various salt concentrations demonstrating the repulsive nature of protein–protein contacts for the halophilic proteins (*Sr* MalDH and *Hm* MalDH) but attractive (or neutral) interactions for the non-halophilic protein (*Tt* LDH and *Ca* MalDH). The slopes were obtained from a linear regression of the S_{exp} data. Pictures: Surface representations of the tetrameric LDH and MalDH enzymes. Top: Electrostatic surface. The electrostatic potential was calculated at 300 K and 0 M salt concentration. Red corresponds to an electrostatic potential smaller than −517 mV. Blue corresponds to a potential greater than 517 mV. The calculated charge densities are −0.004, −0.006, −0.023, and −0.038 e $Å^{-2}$ for *Tt* LDH, *Ca* MalDH, *Sr* MalDH, and *Hm* MalDH, respectively. Bottom: Hydrophobic surface representation. The solvent-accessible hydrophobic surface is colored black. The calculated values are 16,285, 13,811, 9487, and 7384 $Å^2$ for *Tt* LDH, *Ca* MalDH, *Sr* MalDH, and *Hm* MalDH, respectively. The ribbon drawing (green) is shown by transparency.

Author's personal copy

tion of salt in the solvation shell surrounding the protein should be similar to the bulk solvent. High salt strongly modifies the equilibrium between the bulk and the solvation shell, promoting either precipitation or dissolution when either a salting-out or a salting-in salt is added. For a given salt concentration, the tendency of a protein to precipitate (or to stay soluble) is determined by the nature of attractive (or repulsive) weak protein–protein interactions. AUC can be used to determine the dominant regime, because the sedimentation profiles are very sensitive to such interactions.[25] This method has been used previously with success in the study of halophilic proteins.[26] Under high-salt conditions, in which the enzyme is very soluble, the sedimentation coefficient decreases with increasing protein concentration, indicating a repulsive regime.[26] On the other hand, under salt conditions similar to those that promote crystallization of *Hm* MalDH, the sedimentation coefficient increases with protein concentration, indicating that interparticle interactions are under an attractive regime.

We applied this method to study the behavior of the MalDH and LDH enzymes in various KCl concentrations. The experimental sedimentation coefficients were determined using the software SEDFIT[27] (Materials and Methods). To avoid superimposition, we plotted them without correction for density and viscosity, which has no effect on the slope (Fig. 3). The non-halophilic and halophilic enzymes showed opposite behavior (Fig. 3). The non-halophilic enzyme from *Tt* is controlled by a strongly attractive regime at both low and high KCl concentrations (Fig. 3a), and at 3.8 M KCl, the enzyme starts to precipitate at 6–8 mg/ml. The *Ca* MalDH exhibits a more neutral behavior, with small or slightly negative slopes (Fig. 3b). At low salt concentrations, we were able to concentrate *Ca* MalDH to 20–30 mg/ml. In contrast, *Sr* MalDH exhibits a repulsive behavior (Fig. 3c), and at 3.8 M KCl, the protein remains soluble at 35 mg/ml. Due to the limited amount of protein available, we were not able to determine the solubility limit of this enzyme. *Hm* MalDH also exhibits repulsive behavior at high KCl concentrations, and at 4 M NaCl, this enzyme can be concentrated to 200 mg/ml.[17] For probing the relationship between various enzyme surface properties and solubility in more drastic salt conditions, we also measured the AUC profiles in $(NH_4)_2SO_4$ (0.5 and 2.0 M), which typically strongly favors protein precipitation. Halophilic *Sr* MalDH and *Hm* MalDH are still under a repulsive regime and stay soluble (Fig. 3c and d). With *Tt* MalDH, data are very difficult to record at 0.5 and 2.0 M $(NH_4)_2SO_4$, because the *Tt* enzyme precipitates (slowly at 0.5 M and immediately at 2 M). In the case of *Ca* MalDH, the slope indicates a slightly attractive or neutral behavior at low salt concentrations (Fig. 3b). At 2.0 M, $(NH_4)_2SO_4$ data cannot be recorded due to the strong precipitation of the protein.

In a given solvent, differences in protein–protein and protein–solvent interactions between homologous enzymes are mainly due to the nature of the protein surfaces. We therefore analyzed the surfaces of *Tt* LDH and *Ca*, *Sr*, and *Hm* MalDH to determine the structural consequences of the acidic amino acid substitutions in halophilic enzymes. The *Sr* enzyme has about the same number of acidic amino acids oriented toward the solvent (27) as *Hm* (25) and has 14 and 18 more than the *Ca* and *Tt* enzyme, respectively. Of the exposed acidic residues in *Sr* and *Hm* MalDH, 12 are located in identical positions. The qualitative difference between non-halophilic and halophilic enzymes is reflected in the surface electrostatic potential, which is more negative for the halophilic enzymes (Fig. 3, middle row). For the non-halophilic enzymes, the calculated charge density is -0.004 e $Å^{-2}$ for *Tt* MalDH and -0.006 e $Å^{-2}$ for *Ca* MalDH, while it is -0.023 and -0.038 e $Å^{-2}$ for halophilic *Sr* and *Hm* MalDH, respectively.

The solubility should also be impacted by the hydrophobic surface, since the hydrophobic effect is enhanced by high concentrations of neutral salts or by salting-out salts.[3] The total surface area of the tetramer is about the same (within 2% of 41,000 $Å^2$) for each enzyme, but the exposed hydrophobic surface decreases from 38% of the total area in the case of the *Tt* LDH to 33%, 23%, and 18% for the *Ca*, *Sr*, and *Hm* enzymes, respectively (Fig. 3, bottom panels). Our data thus show a strong correlation between the nature of intermolecular interactions (attractive *versus* repulsive) and surface physical properties (electrostatic charge and hydrophobicity).

This suggests that the main adaptive consequence of acidic amino acid substitutions in a halophilic protein favors a change in its intrinsic solubility due to the modification of its surface properties.

The favorable change in enzymatic activity at high salt concentration correlates with subtle structural changes

We measured the effect of KCl on the activity of each enzyme. As expected for non-halophilic enzymes, the activities of *Tt* LDH and *Ca* MalDH were drastically inhibited at KCl concentrations higher than 2 M (Fig. 4a and b). For *Hm* MalDH (Fig. 4d), the activity was maximal over the salt concentration range in which the enzyme is stable (2–4 M). At lower KCl, activity cannot be recorded because the enzyme deactivates.[4] The *Sr* MalDH activity shows an intermediate behavior, as it drops with increasing KCl but still remains at 60% of maximum at high KCl (Fig. 4c).

Structural analysis showed that some structural changes correlate with the increase of activity at

Author's personal copy

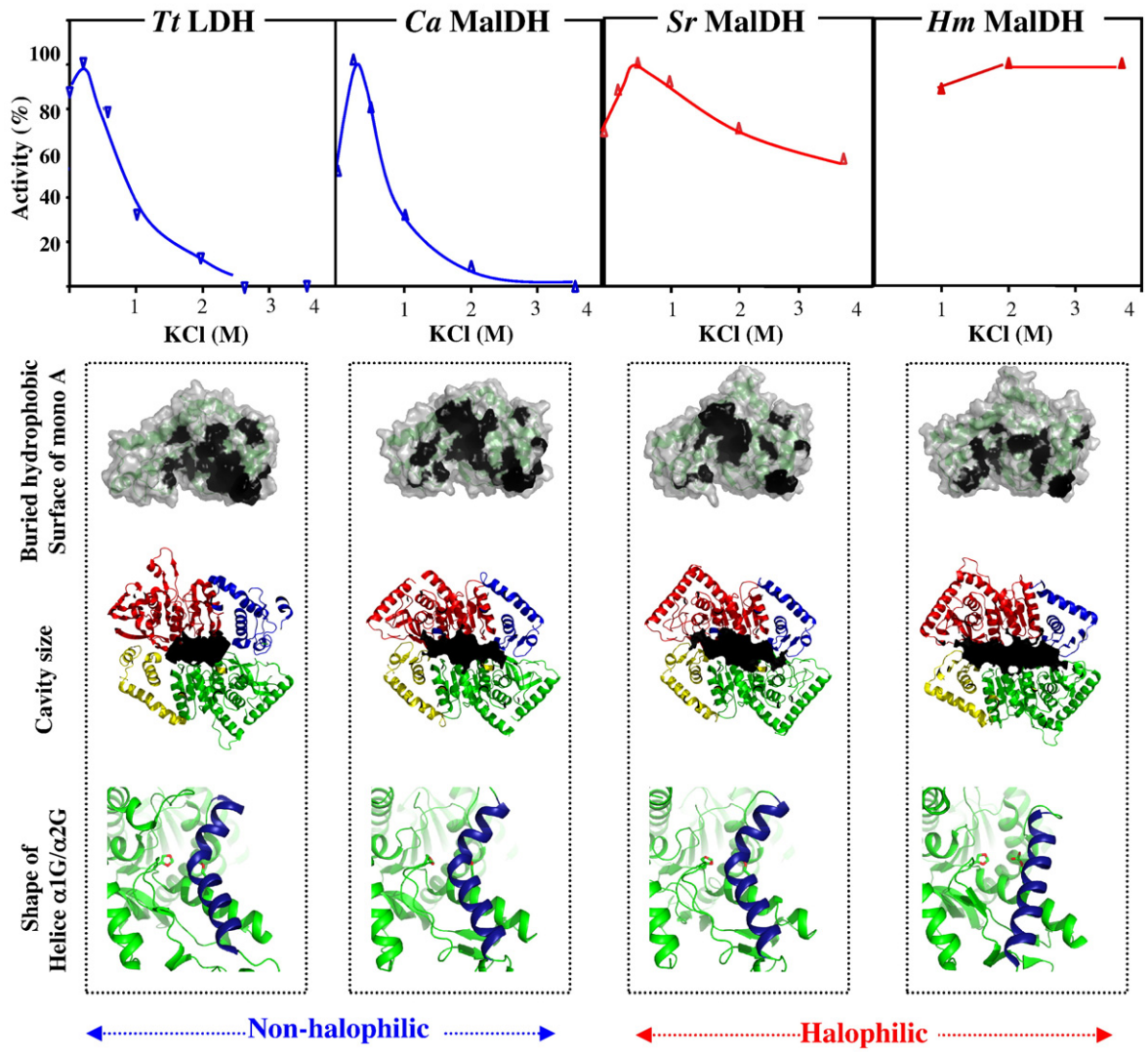

Fig. 4. Graphs: The effect of KCl concentration on the enzymatic activity of *Tt* LDH, *Ca* MalDH, *Sr* MalDH, and *Hm* MalDH. Pictures: Illustrations of structural differences related to activity. Top: Surface contact of monomer A at the monomer–monomer interface that build up the dimer [A–B] or [D–C] (see also Fig. 1). The hydrophobic buried surface area is colored black. The percentage of the hydrophobic surface that contributes to the total buried surface is 60%, 56%, 47%, and 38% for *Tt* LDH, *Ca* MalDH, *Sr* MalDH, and *Hm* MalDH, respectively. Second row: Central cavity (in black) of the enzymes. Calculated volume is 1775, 1602, 2156, and 3516 Å^3 for *Tt* LDH, *Ca* MalDH, *Sr* MalDH, and *Hm* MalDH, respectively. Third row: Close-up view of the catalytic pocket with residues (His195, Arg171, red sticks) involved in catalysis; the backbone is colored green.

high salt concentrations. According to the folding and association pathway of LDH and LDH-like MalDH, the minimal folded unit that sustains activity assembles via the association of monomer A (or D) with monomer B (or C) to build the dimer [A–B] or [D–C].[28] The total surface area of each dimer, as well as the area buried at the dimer interface, is about the same (±5%, not shown). However, the composition of the monomer–monomer interface changes with the enzyme. Specifically, the hydrophobic buried surface represents 60% and 56% of the total buried surface of this interface in the non-halophilic *Tt* LDH and *Ca* MalDH enzymes and decreases to 47% and 38% for *Sr* and *Hm* MalDH, respectively (Fig. 4, second row from top). Assembly of the active dimers that build up the tetramer creates a solvent-accessible cavity (Fig. 4, third row from top). The volume of this cavity increases from an average of 1688 Å^3 for the non-halophilic enzymes to 2156 and 3513 Å^3 for *Sr* and *Hm* MalDH, respectively.

Inside the catalytic vacuole, there are only a few relatively conservative substitutions that are not involved in substrate binding and reactivity and

Author's personal copy

are therefore probably not responsible for the changes in catalytic efficiency. The catalytic mechanism of LDH and MalDH is well understood, following an ordered mechanism in which NADH binds first inside the catalytic vacuole followed by the substrate.[29] In LDH, substrate binding and release induce structural reorganizations of different amplitudes between the apo-state and the ternary complex.[30,31] When switching from the apo-state to the ternary complex, there is a large movement of the catalytic loop and helix αD/E associated with other reorganizations of less importance involving (i) the connecting region between strand βJ and helix α1G and (ii) helix α1G/α2G. In the non-halophilic *Tt* LDH, the connecting region corresponds to a small helix αT, which is shortened in the non-halophilic *Ca* MalDH. In the halophilic *Sr* MalDH, this very small helix superimposes very well with the one observed in *Ca* MalDH (not shown). In *Hm* MalDH, the connecting region βJ–α1G does not contain any secondary elements due to the deletion of few residues. This has a consequence on the location and shape of the α1G/α2G helix, which is in a straight position, allowing the catalytic site to be in a wider open state, a situation that favors substrate trafficking.[32] This phenomenon is not observed in the halophilic *Sr* MalDH enzyme. As observed with its non-halophilic counterparts, the α1G/α2G helix of *Sr* MalDH is kinked (Fig. 4, bottom row). Our data suggest that gradual structural rearrangements promote favorable change of enzymatic activity at high salt concentrations.

Flexibility of the *Sr* MalDH catalytic pocket

One way that the *Sr* enzyme could acquire increased activity at high salt concentrations relative to the *Ca* enzyme would be to increase overall flexibility in the active site region. Because of their effects on local conformational entropy, specific glycine and proline substitutions have been emphasized in adaptive mechanisms within the malate/LDH superfamily.[21,33,34] In cold-adapted LDHs, glycine residues have been selected for mostly in hinge regions that control enzyme conformational flexibility.[21] We found substitutions of non-glycine residue from *Ca* MalDH into glycine residues in *Sr* MalDH. These changes occur mainly in regions surrounding the catalytic pocket that undergo large conformational changes associated with catalysis (Fig. 5a). The conformational entropy is further increased in the *Sr* enzyme relative to the *Ca* one via the removal of Pro at positions 107 and 196 (Fig. 5a).

We also performed a comparison of the refined crystallographic *B*-factors between *Sr* and *Ca* MalDH, using the relative *B*-factor difference at equivalent positions, which limits bias coming from data collection, data integration, and refinement processes. This approach was successful in highlighting the role of three loops in the catalytic process of urate oxidase.[35] Changes in *B*-factors at equivalent

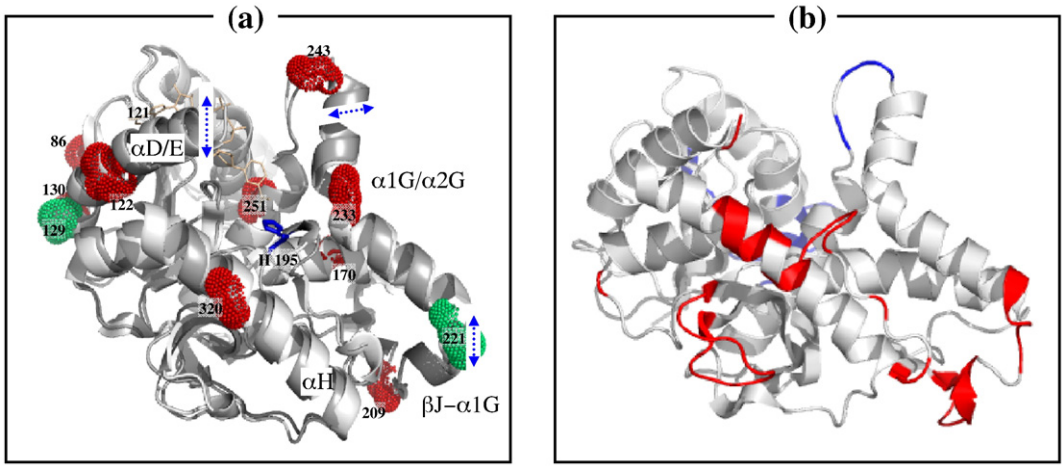

Fig. 5. (a) Ribbon diagram superimposition of *Sr* (gray) and *Ca* MalDH (pale gray). In the *Ca* MalDH structure, the NADH is colored yellow and the catalytic residue H195 is in blue. The blue arrows indicate the main structural differences between the apo-state and the ternary complex of LDH. The locations of additional glycine residues (red balls) in *Sr* MalDH compared to *Ca* MalDH and locations of proline residue (green) in *Ca* MalDH compared to *Sr* MalDH are indicated (PDB numbering). (b) View of the *Ca* MalDH backbone showing in color those residues whose relative crystallographic *B*-factor difference between the *Ca* MalDH and *Sr* MalDH structures is greater than 1 standard deviation with respect to the average value. Red indicates that the *Sr* structure has the higher relative *B*-factor, while blue indicates that the *Ca* structure has the higher relative *B*-factor.

Author's personal copy

positions between the two enzymes convey the effects of amino acid substitutions on protein flexibility, including glycine and proline substitutions as was discussed previously. According to our calculations, there is a net increase of flexibility in *Sr* MalDH compared to *Ca* MalDH (Fig. 5, bottom panel). It should be pointed out that flexibilities of various regions surrounding the catalytic vacuole of *Sr* MalDH are increased, in particular the connecting region βJ–α1G. In the case of LDH, it has been demonstrated that increasing the glycine content in this region permits the enzyme to be more efficient.[31,32]

Discussion

The intermediate nature of the structure and function of *Sr* MalDH offers new insight into molecular halophilic adaptation. The comparison helps to elucidate the specific roles of different types of amino acid substitutions between halophilic and non-halophilic enzymes. The high KCl concentration induces two types of nonspecific effects on enzyme structure and function that are relevant here. First, weak protein–protein interactions tend to become more attractive due to preferential hydration, decreasing protein solubility.[14,16] Second, protein stability is increased not only because of preferential hydration but also because the hydrophobic effect is enhanced in high salt.[36] The increase in stability is thought to freeze out conformational fluctuations required for catalytic activity.[4,5] Thus, the function of a protein placed in a halophilic environment can be improved by (a) increasing solubility and (b) increasing flexibility via decreasing stability, which restores catalytic activity.

With *Sr* and *Hm* MalDH, the solubility problem for the native tetrameric state is solved in two ways. First, the surface is enriched in acidic amino acids, which is well described. About half of the acidic residues occur at the same surface positions, suggesting that either both enzymes had a common halophilic protein ancestor with an intermediate acidic surface (divergent evolution) or there are some specific key surface positions for the location of charge to enhance solubility (convergent evolution). Our comparison and previous studies[14,16,24] show that the acidic enrichment in halophilic proteins enhances both weak (repulsive) interparticle interactions and protein–solvent interactions. Selection of an acidic surface is therefore needed to maintain protein solubility in high salt. Second, by reducing the external hydrophobic surface of the folded protein, hydrophobic protein–protein attraction is also diminished. The reduction in positively charged residues (mainly lysine) sometimes observed in halophilic proteins thus improves solubility by both increasing the net negative surface charge and decreasing the hydrophobic surface area of the folded protein.

In the LDH–MalDH superfamily, solving the activity problem at high salt concentrations is consistent with the notion of stability/activity trade-offs, a phenomenon previously observed in the case of thermal adaptation. Numerous studies suggest that enzymes adapted to high temperatures have reduced activity at lower temperatures because of reduced flexibility.[33,37–39] In terms of the stability/activity landscape, increasing the salt concentration for halo-adaptation corresponds to decreasing the temperature for cold adaptation. High salt concentrations as well as low temperatures decrease the rate at which the enzyme reaches the conformational subset favorable to sustain activity. In both cases, the effects of adaptive substitutions involve increase flexibility, restoring activity to the hyperstabilized enzyme. In the case of LDH-like MalDH, previous studies have shown that the minimal unit that sustains enzymatic activity corresponds to the dimer [A–B] or [D–C].[28,40] Here, our results suggest that the decrease of buried hydrophobic surface between monomers may favor a higher flexibility of the active dimeric unit for the halo-adapted enzymes. We point out, however, that because the native state of oligomeric proteins corresponds to the final step of a complex assembly process requiring the proper folding of intermediates and their association into oligomers, we cannot exclude the effect of the substitutions on this pathway. In particular, substitutions responsible for decreasing the hydrophobic surface between monomers that compose active LDH-like MalDH dimers could have been also selected to prevent improper association due to the high salt concentration. Another potential solution to the activity problem via increased flexibility is with glycine substitutions and decrease of proline content, which has been observed in cold-adapted LDH.[20,31] Although similar changes have occurred in *Sr* MalDH, the sum of these various effects (change of surface composition, decrease of buried hydrophobic interface, and increase of local entropy) is not enough to have fully optimized the enzymatic efficiency of *Sr* MalDH at high salt concentrations, since the activity is still inhibited by 50% compared to its maximal activity achieved at low salt concentration.

Our work suggests that the evolutionary process of proteins adapting to high salt concentrations is an "ordered/sequential" trade-off between activity, solubility, and stability to counterbalance the unfavorable effect of high salt concentrations on enzyme conformational landscape fluctuations. In the first step of halo-adaptation, sequence changes are selected to favor solubility and partially prevent salt inhibition. The activity at high salt concentrations can then be improved, further reducing stability and correspondingly increasing the flexibility required for catalysis.

Author's personal copy

Materials and Methods

Sample preparation

Purifications of *Sr*, *Ca*, and *Hm* MalDH and *Tt* LDH enzymes were carried out as previously reported.[6,19–21] Protein concentrations were determined from the absorbance at 280 nm using extinction coefficients calculated from the sequence of each protein†.

Conformational stability

Residual circular dichroism (CD) and residual activity were used to determine conformational stability.[28] The proteins of interest were incubated for 24 h at 0.1 mg/ml in various KCl concentrations prior to performing CD and activity assays.

Standard enzymatic assay

The activity was determined by following the oxidation of NADH over 30 s by measuring the decrease in absorbance at 340 nm (Beckman DU 7500 Spectrophotometer). For MalDH, the measurements were performed at 60 °C (near the optimal temperature for each enzyme) using saturating concentrations of the substrate oxaloacetate (OAA) to avoid artifacts from K_m variation due to high salt concentrations.[4] For the measurements on *Tt* LDH, the temperature was set to 75 °C and the substrate was pyruvate instead of OAA. Enzyme aliquots were mixed with 1 ml of 50 mM Tris–HCl, pH 8.0, supplemented with OAA (0.3 mM) or pyruvate (0.3 mM) and NADH (0.2 mM) at various salt concentrations.

Sedimentation velocity measurement

Sedimentation velocity experiments were performed with a Beckman XLI analytical ultracentrifuge, equipped with a UV scanning system, using an eight-hole AN-60 Ti rotor with a double-channel centerpiece of 1.2 cm optical path length. For each sample, 200 absorbance profiles were recorded at 280 nm (*Tt* LDH, *Sr* MalDH, and *Hm* MalDH) or 275 nm (*Ca* MalDH) at 42,000 RPM, at 20 °C after a temperature equilibration of 2 h. At a protein concentration close to 3 mg/ml, data were also recorded at 250 nm to avoid optical saturation artifacts. The experimental sedimentation coefficients were determined using the continuous size distributions $c(s)$ option in the SEDFIT software.[27] The data were fitted over the range of 0.1 to 15 s with a resolution grid of 200 points and systematic noise subtraction. The sedimentation profiles were well fit with a single component (>95% of the signal) and some discrete non-interacting species, which are considered to be contaminants. The experimental S value was obtained by the weight-average S value of the main sharp-distribution peak. Because the analyzed enzymes are homologous and display a globular shape, we assume that they have a same partial specific volume of 0.74 and friction coefficient f/f_0 of 1.20. In the case of *Hm* MalDH, this last assumption is only valid at high salt concentrations in which the enzyme is stable. According to SEDFIT specifications, under optimal conditions, the S values are given with errors of ±0.4%. We assume that, in most of our experiments, the small RMSD and low residual variation of ±0.015 optical density permitted us to determine S values with an uncertainty of ±1%. The $c(s)$ analysis within such confident limits was shown to be very satisfactory to characterize halophilic *Hm* MalDH in complex solvents[26] and to probe the behavior of an elongated protein in concentrated salt solution.[41]

Crystallization and structure determination of *Sr* MalDH

Crystals were grown at room temperature using the hanging-drop vapor-diffusion method. *Sr* MalDH protein (11 mg/ml in 50 mM Tris–HCl, pH 8) was mixed with an equal volume (2 µl) of mother liquor of 1 M LiCl, pH 4.0, 0.1 M citric acid, and 10% polyethylene glycol 6000. The crystal was soaked into a cryo-protective buffer [mother liquor containing 20% (v/v) added glycerol] before being flash-cooled in a nitrogen vapor stream at 100 K. Diffraction data were collected to a resolution of 1.55 Å at beam line BM30 of the European Synchrotron Radiation Facility (ESRF). Ice rings at resolutions of 2.2 and 1.9 Å were visible in diffraction frames and reflections in these resolution ranges were excluded. A second crystal was soaked in a slightly different cryo-protectant buffer [mother liquor containing 25% (v/v) added glycerol] and diffraction data were recorded to a resolution of 1.8 Å at ESRF beam line ID29. Diffraction data frames from each data set were indexed and integrated with the program XDS. As the crystals were isomorphous (a difference of 0.1%, 0.4%, and 0.3% in cell parameters was observed for a, b, and c, respectively), the two data sets were scaled and merged using the program XSCALE in space group $I222$ with cell dimensions of 76.11, 87.72, and 100.45 Å. Structure factor amplitudes were derived using the program XDSCONV[42] (Table 1). The asymmetric unit content was estimated as a single subunit via the calculation of the Matthews coefficient.[43]

The three-dimensional structure was determined using the molecular replacement method with the program PHASER[44] (v 1.3.3) and diffraction data in the resolution range 40–3 Å. The search model was a monomer of *Chlorobium tepidum* MalDH [Protein Data Bank (PDB) code 1GUZ] and a unique solution was found with a Z-factor of 26.3 (LL gain of 613). After a rigid-body refinement using data in the resolution 40–3 Å, an initial R-factor of 42% was obtained. Subsequent refinement process consisted of energy minimization and individual anisotropic B factor refinement for protein atoms and isotropic B-factor refinement for solvent atoms using the complete set of recorded reflections using the program PHENIX[45] (v 1.6_288). The model was built with Coot[46] between refinement cycles. The current refined atomic model comprises 306 residues and 340 water molecules. The homotetrameric molecule that corresponds to the biological assembly can be generated by the crystal symmetry operators of the $I222$ space group. The quality

† http://www.expasy.ch/tools/protparam.html

Author's personal copy

of the model was checked using the MolProbity server[47] (Table 1). The numbering of *Sr* MalDH model is based on that of *Hm* MalDH and the Eventoff nomenclature.[48]

Model analysis

The model of *Sr* MalDH was compared to the structures of the halophilic *Hm* MalDH (PDB code 1GT2) and of the non-halophilic *Ca* MalDH (PDB code 1GUY) and *Tt* LDH (PDB code 2V6M). Residue numbering of *Ca* MalDH in this article is based on *Sr* MalDH numbering and differs from that of the initial PDB. The solvent-accessible surface area of all tetrameric MalDHs was calculated using the program AREAIMOL.[49] For each tetramer, interfaces between monomers were examined with the program PISA.[50] The probe-accessible volume of the central cavities was calculated using the program VOIDOO.[51] The probe radius was set to 1.4 Å (i.e., water radius) and the central cavity was specifically selected with coordinates of a cavity point. The electrostatic potential was generated with the program APBS[52] and rendered with PyMOL (PyMOL Molecular Graphics System, Version 1.2r3pre, Schrödinger, LLC), which was also used to prepare all the figures. The relative crystallographic *B*-factor difference for each residue was calculated for the backbone atoms using the formula $\frac{(B_{Ca} - \langle B_{Ca}\rangle) - (B_{Sr} - \langle B_{Sr}\rangle)}{\langle B_{Ca}\rangle - \langle B_{Sr}\rangle}$, where B_{Ca} and B_{Sr} refer to *B*-factor values extracted from *Ca* and *Sr* MalDH models, respectively, and where $\langle B\rangle$ refers to the mean value for the whole structure. This calculation leads to a distribution with a zero mean value and limits bias from refinements. The *Sr* MalDH sequence was aligned to the sequence from *Ca* MalDH.

Accession numbers

Coordinates and structure factors have been deposited in the PDB with accession number 3NEP.

Acknowledgements

We thank Dr Giuseppe Zaccai for helpful discussions and critical reading of the manuscript. Financial support by the Centre National de la Recherche Scientifique [Project EOPV (Environnements Planétaires et Origines de la Vie)] is acknowledged.

References

1. Oren, A. (2002). Halophilic microoganisms and their environments. In *Cellular Origin and Life in Extreme Environments* Kluwer Academic Publishers, Dordrecht, The Netherlands.
2. Antón, J., Oren, A., Benlloch, S., Rodríguez-Valera, F., Amann, R. & Rosselló-Mora, R. (2002). *Salinibacter ruber* gen. nov., sp. nov., a novel, extremely halophilic member of the *Bacteria* from saltern crystallizer ponds. *Int. J. Syst. Evol. Microbiol.* **52**, 485–491.
3. Timasheff, S. N. (1991). Solvent effect on protein stability. *Curr. Opin. Struct. Biol.* **2**, 35–39.
4. Madern, D., Ebel, C. & Zaccai, G. (2000). Halophilic adaptation of enzymes. *Extremophiles*, **4**, 91–98.
5. Mevarech, M., Frolow, F. & Gloss, L. M. (2000). Halophilic enzymes: proteins with a grain of salt. *Biophys. Chem.* **86**, 155–164.
6. Bonneté, F., Madern, D. & Zaccai, G. (1994). Stability against denaturation mechanisms in halophilic malate dehydrogenase "adapt" to solvent conditions. *J. Mol. Biol.* **244**, 436–447.
7. Richard, S. B., Madern, D., Garcin, E. & Zaccai, G. (2000). Halophilic adaptation: novel solvent protein interactions observed in the 2.9 and 2.6 Å resolution structures of the wild type and a mutant of malate dehydrogenase from *Haloarcula marismortui*. *Biochemistry*, **39**, 992–1000.
8. Bieger, B., Essen, L. O. & Oesterhelt, D. (2003). Crystal structure of halophilic dodecin. A novel dodecameric flavin binding protein from *Halobacterium salinarum*. *Structure*, **4**, 375–385.
9. Britton, K. L., Baker, P. J., Fisher, M., Ruzheinikov, S., Gilmour, D. J., Bonete, M. J. *et al.* (2006). Analysis of protein solvent interactions in glucose dehydrogenase from the extreme halophile *Haloferax mediterranei*. *Proc. Natl Acad. Sci. USA*, **103**, 4846–4851.
10. Paul, S., Bag, S. K., Das, S., Harvill, E. T. & Dutta, C. (2008). Molecular signature of hypersaline adaptation: insights from genome and proteome composition of halophilic prokaryotes. *Genome Biol.* **9**, R70.
11. Wende, A., Johansson, P., Vollrath, R., Dyall-Smith, M., Oesterhelt, D. & Grininger, M. (2010). Structural and biochemical characterization of a halophilic archaeal alkaline phosphatase. *J. Mol. Biol.* **400**, 52–62.
12. Tadeo, X., López-Méndez, B., Trigueros, T., Laín, A., Castaño, D. & Millet, O. (2009). Basis for the aminoacid composition of proteins from halophilic archea. *PLoS Biol.* **7**, e1000257.
13. Madern, D. (2002). Molecular evolution within the L-malate and L-lactate dehydrogenase super-family. *J. Mol. Evol.* **54**, 825–840.
14. Ebel, C., Costenaro, L., Pascu, M., Faou, P., Kernel, B., Proust-De Martin, F. & Zaccai, G. (2002). Solvent interactions of halophilic malate dehydrogenase. *Biochemistry*, **41**, 13234–13244.
15. Ebel, C., Faou, P., Kernel, B. & Zaccai, G. (1999). The relative role of anions and cations in the stabilization of halophilic malate dehydrogenase. *Biochemistry*, **38**, 9039–9047.
16. Costenaro, L., Zaccai, G. & Ebel, C. (2002). Link between protein–solvent and weak protein–protein interactions gives insight into halophilic adaptation. *Biochemistry*, **41**, 13245–13252.
17. Bonneté, F., Ebel, C., Zaccai, G. & Eisenberg, H. (1993). Biophysical study of halophilic malate dehydrogenase in solution: revised subunit structure and solvent interactions of native and recombinant enzyme. *J. Chem. Soc., Faraday Trans.* **89**, 2659–2666.
18. Irimia, A., Ebel, C., Madern, D., Richard, S. B., Cosenza, L. W., Zaccai, G. & Vellieux, F. M. (2003). The oligomeric state of *Haloarcula marismortui* malate dehydrogenase are modulated by solvent components as shown by crystallographic and biochemical studies. *J. Mol. Biol.* **326**, 859–873.

Author's personal copy

19. Dalhus, B., Saarinen, M., Sauer, U. H., Eklund, P., Johansson, K., Karlsson, A. *et al.* (2002). Structural basis for thermophilic protein stability: structures of thermophilic and mesophilic malate dehydrogenases. *J. Mol. Biol.* **318**, 707–721.
20. Madern, D. & Zaccai, G. (2004). Molecular adaptation: the malate dehydrogenase from the extreme halophilic bacterium *Salinibacter ruber* behaves like a non-halophilic protein. *Biochimie*, **86**, 295–303.
21. Coquelle, N., Fioravanti, E., Weik, M., Vellieux, F. & Madern, D. (2007). Activity, stability and structural studies of lactate dehydrogenases adapted to extreme thermal environments. *J. Mol. Biol.* **374**, 547–562.
22. Madern, D. & Ebel, C. (2007). Influence of an anion-binding site in the stabilization of halophilic malate dehydrogenase from *Haloarcula marismortui*. *Biochimie*, **89**, 981–987.
23. Olsher, U., Izatt, R. M., Bradshaw, J. S. & Dalley, N. K. (1991). Coordination chemistry of lithium ion, a crystal and molecular structure review. *Chem. Rev.* **91**, 137–164.
24. Tardieu, A, Bonneté, F., Finet, S. & Vivarès, D. (2002). Understanding salt or PEG induced attractive interactions to crystallize biological macromolecules. *Acta Crystallogr., Sect. D.: Biol. Crystallogr.* **58**, 1549–1553.
25. Behlke, J. & Ristau, O. (1999). Analysis of the thermodynamic non-ideality of proteins by sedimentation equilibrium experiments. *Biophys. Chem.* **76**, 13–23.
26. Solovyova, A., Schuck, P., Costenaro, L. & Ebel, C. (2001). Non-ideality by sedimentation velocity of halophilic malate dehydrogenase in complex solvents. *Biophys. J.* **81**, 1868–1880.
27. Schuck, P. (2000). Size-distribution analysis of macromolecules by sedimentation velocity ultracentrifugation and Lamm equation modeling. *Biophys. J.* **78**, 1606–1619.
28. Madern, D., Ebel, C., Mevarech, M., Richard, S. B., Pfister, C. & Zaccai, G. (2000). Insights into the molecular relationships between malate and lactate dehydrogenases. Structural and biochemical properties of monomeric and dimeric intermediates of a mutant of tetrameric LDH-like malate dehydrogenase from the halophilic archaeon *Haloarcula marismortui*. *Biochemistry*, **39**, 1001–1010.
29. Holbrook, J. J., Lilias, A., Steindel, S. J. & Rossmann, M. G. (1975). Lactate dehydrogenase. In *The Enzymes* (Boyer, P. D., ed.), pp. 191–292, Academic Press, New York, NY.
30. Gerstein, M. & Chothia, C. (1991). Analysis of protein loop closure. Two types of hinges produce one motion in lactate dehydrogenase. *J. Mol. Biol.* **220**, 133–149.
31. Iwata, S., Kamata, K., Yoshida, S., Minowa, T. & Ohta, T. (1994). T and R states in the crystals of bacterial L-lactate dehydrogenase reveal the mechanism for allosteric control. *Nat. Struct. Biol.* **1**, 176–185.
32. Dym, O., Mevarech, M. & Sussman, J. L. (1995). Structural features that stabilize halophilic malate dehydrogenase from an archaebacterium. *Science*, **267**, 1344–1346.
33. Fields, P. A. & Somero, G. N. (1999). Hot spots in cold adaptation: localized increases in conformational flexibility in lactate dehydrogenase A4 orthologs of Antarctic notothenioid fishes. *Proc. Natl Acad. Sci. USA*, **95**, 11476–11481.
34. Johns, G. C. & Somero, G. N. (2004). Evolutionary convergence in adaptation of proteins to temperature: A4-lactate dehydrogenases of Pacific damselfishes. *Mol. Biol. Evol.* **2**, 314–320.
35. Girard, E., Marchal, S., Perez, J., Finet, S., Kahn, R., Fourme, R. *et al.* (2010). Structure–function perturbation and dissociation of tetrameric urate oxidase by high hydrostatic pressure. *Biophys. J.* **98**, 2365–2373.
36. Thomas, A. S. & Elcock, A. H. (2006). Direct observation of salt effects on molecular interactions through explicit-solvent molecular dynamics simulations: differential effects on electrostatic and hydrophobic interactions and comparisons to Poisson–Boltzmann theory. *J. Am. Chem. Soc.* **128**, 7796–7806.
37. Collins, T., Meuwis, M. A., Gerday, C. & Feller, G. (2003). Activity, stability and flexibility in glycosidases adapted to extreme thermal environments. *J. Mol. Biol.* **328**, 419–428.
38. Georlette, D., Damien, B., Blaise, V., Depiereux, E., Uversky, V. N., Gerday, C. & Feller, G. (2003). Structural and functional adaptations to extreme temperatures in psychrophilic, mesophilic, and thermophilic DNA ligases. *J. Biol. Chem.* **278**, 37015–37023.
39. Bae, E. & Phillips, G. N., Jr. (2004). Structures and analysis of highly homologous psychrophilic, mesophilic, and thermophilic adenylate kinases. *J. Biol. Chem.* **279**, 28202–28208.
40. Madern, D., Ebel, C., Dale, H. A., Lien, T., Steen, I. H., Birkeland, N. K. & Zaccai, G. (2001). Differences in the oligomeric states of the LDH-like L-MalDH from the hyperthermophilic archaea *Methanococcus jannaschii* and *Archaeoglobus fulgidus*. *Biochemistry*, **40**, 10310–10316.
41. Okemefuna, A. I., Nan, R., Gor, J. & Perkins, S. J. (2009). Electrostatic interactions contribute to the folded-back conformation of wild type human factor H. *J. Mol. Biol.* **391**, 98–118.
42. Kabsch, W. (1993). Automatic processing of rotation diffraction data from crystals of initially unknown symmetry and cell constants. *J. Appl. Crystallogr.* **26**, 795–800.
43. Matthews, B. W. (1968). Solvent content of protein crystals. *J. Mol. Biol.* **33**, 491–497.
44. McCoy, A. J., Grosse-Kunstleve, R. W., Storoni, L. C. & Read, R. J. (2005). Likelihood-enhanced fast translation functions. *Acta Crystallogr., Sect. D.: Biol. Crystallogr.* **61**, 458–464.
45. Adams, P. D., Afonine, P. V., Bunkóczi, G., Chen, V. B., Davis, I. W., Echoo, N. *et al.* (2010). PHENIX: a comprehensive Python-based system for macromolecular structure solution. *Acta Crystallogr., Sect. D.: Biol. Crystallogr.* **66**, 213–221.
46. Emsley, P., Lohkamp, B., Scott, W. G. & Cowtan, W. (2010). Features and development of Coot. *Acta Crystallogr., Sect. D.: Biol. Crystallogr.* **66**, 486–501.
47. Chen, V. B. W., Arendall, B., Headd, J. J., Keedy, D. A., Immormino, R. M., Kapral, G. J. *et al.* (2010). MolProbity: all-atom structure validation for macromolecular crystallography. *Acta Crystallogr., Sect. D.: Biol. Crystallogr.* **66**, 12–21.
48. Eventoff, W., Rossmann, M. G., Taylor, S. S., Torff, H. J., Meyer, H., Keil, W. & Kiltz, H. H. (1977). Structural

Author's personal copy

adaptations of lactate dehydrogenase isozymes. *Proc. Natl Acad. Sci. USA*, **74**, 2677–2681.
49. Saff, E. B. & Kuijlaars, A. B. J. (1997). Distributing many points on a sphere. *Math. Intell.* **19**, 5–11.
50. Krissinel, E. & Henrick, K. (2007). Inference of macromolecular assemblies from crystalline state. *J. Mol. Biol.* **372**, 774–797.
51. Kleywegt, G. J. & Jones, T. A. (1994). Detection, delineation, measurement and display of cavities in macromolecular structures. *Acta Crystallogr., Sect. D.: Biol. Crystallogr.* **50**, 178–185.
52. Baker, N. A., Sept, D., Joseph, S., Holst, M. J. & McCammon, J. A. (2001). Electrostatics of nanosystems. *Proc. Natl Acad. Sci. USA*, **98**, 10037–10141.